THE JOURNAL OF PHYSICAL CHEMISTRY A

Article

pubs.acs.org/JPCA

Monohafnium Oxide Clusters HfO_n^- and HfO_n (n = 1−6): Oxygen Radicals, Superoxides, Peroxides, Diradicals, and Triradicals

Hua-Jin Zhai,[†] Wen-Jie Chen,[‡] Shu-Juan Lin,[‡] Xin Huang,*[,‡] and Lai-Sheng Wang*[,†]

[†]Department of Chemistry, Brown University, Providence, Rhode Island 02912, United States

[‡]Department of Chemistry, Fuzhou University, Fuzhou, Fujian 350108, P. R. China

ABSTRACT: The electronic and structural properties of monohafnium oxide clusters, HfO_n^- and HfO_n (n = 1−6), are investigated using anion photoelectron spectroscopy and density-functional theory at the B3LYP level. The observed ground-state adiabatic detachment energy is low for HfO^- (0.5 ± 0.1 eV) and HfO_2^- (2.125 ± 0.010 eV), roughly constant for HfO_3^- (3.6 ± 0.1 eV), HfO_4^- (3.67 ± 0.05 eV), and HfO_5^- (3.9 ± 0.1 eV), and substantially higher for HfO_6^- (4.9 ± 0.1 eV). Activated oxygen species, such as radical, superoxide, peroxide, diradical, and triradical, are identified in the HfO_n^- and HfO_n clusters. The Hf center is shown to be flexible to accommodate the oxygen species. The sum of formal Hf−O bond orders around the Hf center is equal to four for all of the neutral clusters studied, and five for all of the anions. The O-rich HfO_n^- and HfO_n (n = 3−6) clusters provide well-defined molecular models to understand O_2 adsorption and activation on an Hf center.

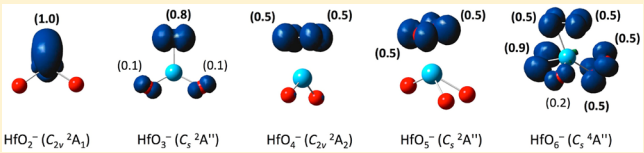

I. INTRODUCTION

How a metal center interacts with oxygen species is relevant to the surface chemistry of transition metal oxides.[1] Gas-phase oxide clusters serve as well-defined molecular models for metal oxide surfaces and can provide mechanistic insights to surface chemical reactions.[2−21] Among early transition metal oxides, those of group IVB elements (Ti, Zr, and Hf) are involved in numerous technological applications. For example, HfO_2 embedded in a carbon matrix can catalyze the aromatization of C_{6+} alkanes,[22] whereas TiO_2 is a prototypical photocatalyst.[23] However, gas-phase spectroscopic data for these early transition metal oxides have been relatively scarce.[7,13,15,24] Furthermore, Hf oxide clusters represent valuable molecular models pertinent to the understanding of defect sites in HfO_2 bulk oxides and thin films, which are being considered as the leading candidate for the next generation high-κ gate insulator to replace SiO_2 in field effect transistors due to their high dielectric constant.[25]

There have been a few previous studies on gas-phase Hf oxide clusters. Early electron impact measurements yielded the ionization potentials of 7.5 ± 0.1 and 9.3 ± 0.2 eV for HfO and HfO_2, respectively.[26] Matrix isolation infrared (IR) spectroscopic studies[27] allowed the identification of the HfO, HfO_2, Hf_2O_2, and Hf_2O_4 species. A subsequent matrix IR study characterized the O-rich species such as $OHf(O_2)(O_3)$, $Hf(O_2)_3$, and $Hf(O_2)_4$.[28] Rotational spectra of jet-cooled HfO and HfO_2 were reported recently,[29] yielding a C_{2v} ground state for HfO_2 with an Hf−O bond distance of 1.7764 ± 0.0004 Å and ∠OHfO bond angle of 107.51 ± 0.01°, and a bond distance of 1.7231481 Å for the diatomic HfO species. Photoelectron spectroscopy (PES) was used to study HfO_2^- at a detachment energy of 355 nm, yielding the electron affinity (EA) of HfO_2 to be 2.14 ± 0.03 eV.[30] Two comparative theoretical studies on $(MO_2)_n$ (M = Ti, Zr, Hf) clusters were carried out at the density-functional theory (DFT) and coupled-cluster [CCSD(T)] levels.[31,32] In particular, the extensive computational data at the CCSD(T) level were used to calibrate the performance of the DFT methods on the electronic and structural properties of the $(HfO_2)_n$ clusters.[32]

In the current contribution, we report a joint study on a series of monohafnium oxide clusters, HfO_n^- and HfO_n (n = 1−6), using anion PES and DFT calculations at the B3LYP level. The ground-state adiabatic detachment energy (ADE) is shown to increase monotonically for HfO^- (0.5 ± 0.1 eV), HfO_2^- (2.125 ± 0.010 eV), and HfO_3^- (3.6 ± 0.1 eV); it remains roughly constant for HfO_3^-, HfO_4^- (3.67 ± 0.05 eV), and HfO_5^- (3.9 ± 0.1 eV) and becomes substantially higher for HfO_6^- (4.9 ± 0.1 eV). The global minimum structures are determined via comparison between experiment and theory, and a variety of activated oxygen species such as radical, superoxide, peroxide, diradical, and triradical are identified. The Hf center appears to be highly flexible to accommodate oxygen species, where the sum of the formal Hf−O bond orders around the Hf center is equal to four and five, respectively, for the neutral and anion clusters. The O-rich HfO_n^- and HfO_n (n = 3−6) clusters serve as valuable molecular models for O_2 adsorption and activation on the Hf center.

II. EXPERIMENTAL AND COMPUTATIONAL METHODS

A. Photoelectron Spectroscopy. The experiment was carried out using a magnetic-bottle PES apparatus equipped with a laser vaporization cluster source, details of which were described previously.[33] Briefly, $Hf_mO_n^-$ anion clusters were produced by laser vaporization of a pure Hf disk target in the

Special Issue: Peter B. Armentrout Festschrift

Received: March 24, 2012
Revised: June 5, 2012
Published: June 6, 2012

presence of a helium carrier gas seeded with 0.01−0.5% O_2 and analyzed using a time-of-flight mass spectrometer. The HfO_n^- (n = 1−6) clusters of interest were each mass-selected and decelerated before being photodetached at 193 nm (6.424 eV) from an ArF excimer laser. Additional higher resolution experiment was performed for HfO_2^- at 355 nm (3.496 eV) from a Nd:YAG laser. Effort was made to control the cluster temperatures and to choose colder clusters for the PES experiment, which was shown previously to be critical for obtaining high quality PES data.[34] Photoelectrons were collected at nearly 100% efficiency by the magnetic bottle and analyzed in a 3.5 m long electron flight tube. The PES spectra were calibrated using the known spectra of Au^- and Rh^-. The energy resolution of the apparatus was $\Delta E_k/E_k \approx$ 2.5%, that is, ∼25 meV for 1 eV electrons.

B. Computational Methods. The DFT calculations were carried out using the B3LYP hybrid functional.[35−37] Global minimum searches were performed using analytical gradients with the Stuttgart relativistic small core basis set and efficient core potential[38,39] augmented with two f-type and one g-type polarization functions for Hf [$\zeta(f)$ = 0.163, 0.557; $\zeta(g)$ = 0.352] as recommended by Martin and Sundermann[40] and the aug-cc-pVTZ basis set for oxygen.[41,42] Scalar relativistic effects, that is, the mass velocity and Darwin effects, were taken into account via the quasi-relativistic pseudopotentials. Vibrational frequency calculations were done to verify the nature of the stationary points, and all structures presented herein are true minima on the potential energy surfaces. Vertical detachment energies (VDEs) were calculated using the generalized Koopmans' theorem by adding a correction term to the eigenvalues of the anion.[43] The correction term was calculated as $\delta E = E_1 - E_2 - \varepsilon_{HOMO}$, where E_1 and E_2 are the total energies of the anion and neutral, respectively, in their ground states at the anion equilibrium geometry and ε_{HOMO} corresponds to the eigenvalue of the highest occupied molecular orbital (HOMO) of the anion. All calculations were performed using the Gaussian 03 package.[44]

III. EXPERIMENTAL RESULTS

The PES spectra of HfO_n^- (n = 1−6) clusters taken at 193 nm (6.424 eV) are shown in Figures 1−3. The 355 nm spectrum of

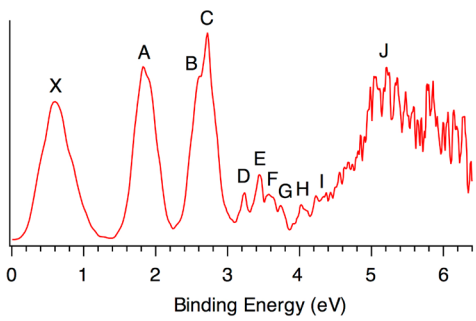

Figure 1. Photoelectron spectrum of HfO^- at 193 nm (6.424 eV).

HfO_2^- with rich vibrational structures is also obtained (Figure 2a). The observed spectral bands are labeled with letters (X, A−J) and the measured ADEs and VDEs are summarized in Tables 1 and 2, where the ground-state VDEs are compared with those calculated from the lowest-energy and low-lying anion structures at the B3LYP level.

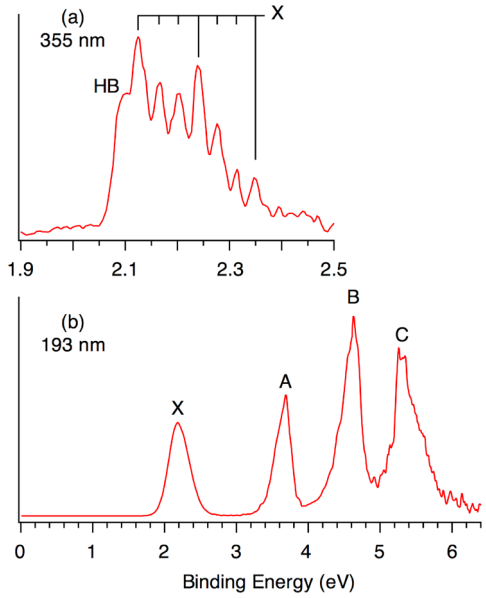

Figure 2. Photoelectron spectra of HfO_2^- at (a) 355 nm (3.496 eV) and (b) 193 nm. The vertical lines represent the resolved vibrational structures for the ground-state transition. HB stands for a hot band transition.

A. HfO^-. The 193 nm PES spectrum of HfO^- (Figure 1a) shows numerous detachment transitions, among which eleven bands are identified (X, A−J). The ground-state VDE is measured from the maximum of band X to be 0.60 eV (Table 1). The ground-state ADE, 0.5 ± 0.1 eV, is estimated by drawing a straight line along the leading edge of band X and then adding the instrumental resolution to the intersection with the binding energy axis. The ground-state ADE also represents the EA of neutral HfO. Bands A (1.8 eV), B (2.6 eV), and C (2.8 eV) all show strong relative intensities. Between 3.1 and 4.5 eV, a series of closely spaced weak bands (D−I) are observed, beyond which continuous spectral features are observed. A band J is labeled at ∼5.2 eV for the sake of discussion.

B. HfO_2^-. The 193 nm PES spectrum of HfO_2^- (Figure 2b) reveals four well-separated bands. The ground-state transition (X) is accessible at 355 nm, which yields a vibrationally resolved spectrum with two vibrational progressions (Figure 2a). The frequencies of the two modes are measured to be 890 ± 30 and 290 ± 30 cm^{-1}. A hot band transition (HB) is also partially resolved at the low binding energy side, yielding a vibrational frequency of ∼250 cm^{-1} for the ground state of HfO_2^-. The 0−0 transition at 2.125 ± 0.010 eV defines both the ground-state ADE and VDE for HfO_2^-, which is also the EA of neutral HfO_2. A prior PES measurement at 355 nm gave an EA of 2.14 ± 0.03 eV and vibrational frequency (887 ± 40 cm^{-1}) for HfO_2, but the low frequency mode was not resolved.[30] Our 193 nm spectrum reveals three more higher energy bands with VDEs: A (3.68 eV), B (4.63 eV) and C (5.30 eV). The ADE for band A is evaluated as 3.44 ± 0.10 eV. The ADE difference between bands X and A defines an excitation energy of 1.3 eV, which also represents the HOMO−LUMO gap for HfO_2.

C. HfO_n^- (n = 3−6). The PES spectrum of HfO_3^- (Figure 3a) shows three bands with VDEs: X (3.82 eV), A (4.55 eV), and B (5.44 eV). The VDEs of these bands are similar to those of the A, B, C bands of HfO_2^-, respectively. The PES spectrum

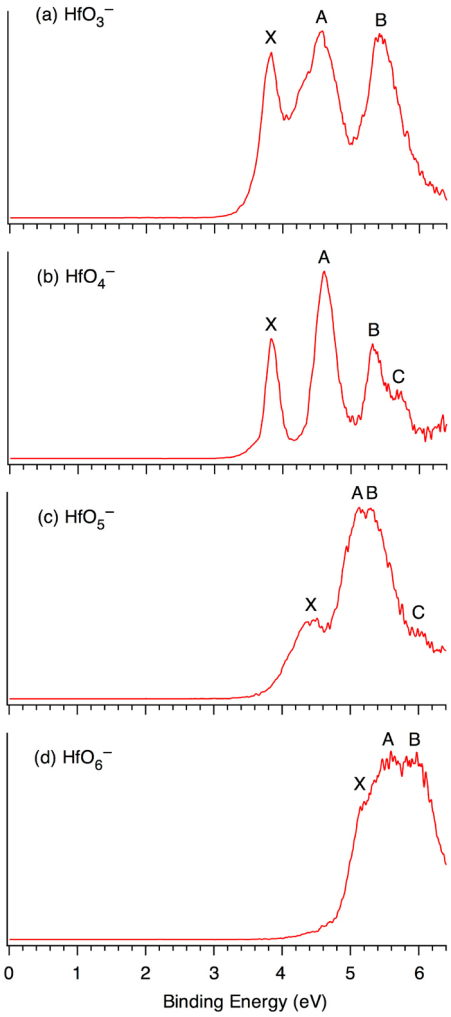

Figure 3. Photoelectron spectra of HfO_n^- (n = 3−6) clusters at 193 nm.

for HfO_4^- (Figure 3b) is relatively sharp, showing four well resolved bands with VDEs: X (3.84 eV), A (4.61 eV), B (5.34 eV), and C (5.71 eV). The PES spectra for HfO_5^- (Figure 3c) and HfO_6^- (Figure 3d) are broad and show overlapping bands. Four bands (X, 4.43 eV; A, 5.14 eV; B, 5.30 eV; C, 6.00 eV) are tentatively labeled for HfO_5^-, whereas three bands (X, 5.32 eV; A, 5.57 eV; B, 5.88 eV) are labeled for HfO_6^-.

Note that many of the PES bands for the HfO_n^- clusters are quite broad, hinting significant geometry changes between the anions and the neutral states or multiple electronic transitions. In the latter cases, the VDEs reported in Table 2 should be considered as the average of the multiple transitions. The ground-state ADEs of HfO_n^- (n = 3−6) are estimated from the onset of the band X to be 3.6 ± 0.1, 3.67 ± 0.05, 3.9 ± 0.1, and 4.9 ± 0.1 eV, respectively (Table 2).

IV. THEORETICAL RESULTS

The optimized structures for the HfO_n^- and HfO_n (n = 2−6) clusters are depicted in Figure 4. The HfO^- anion possesses a $C_{\infty v}$ ($^2\Delta$) ground state with a bond distance of 1.780 Å, whereas the HfO neutral adopts a $C_{\infty v}$ ($^1\Sigma^+$) ground state with a slightly shortened bond distance of 1.729 Å, in close agreement with that deduced from the rotational spectroscopy (1.7231481 Å).[29] These calculated distances should be assigned as Hf═O double bonds, although that in the neutral in

Table 1. Experimental Adiabatic (ADE) and Vertical (VDE) Detachment Energies and Term Values (T_e) from the Photoelectron Spectrum of HfO^-, Compared to the Term Values of HfO from Prior High-Resolution Optical Spectroscopy (ref 49)

feature	final state[a]	ADE (eV)[b]	T_e (eV)	VDE (eV)[b]	T_e (eV) (ref 49)
X	$^1\Sigma^+$	0.5 (1)[c]	0.00	0.6 (1)[d]	0.000 ($^1\Sigma^+$)
					1.144 ($^3\Delta_1$)
A	$^3\Delta$	1.7 (1)	1.2	1.8 (1)[e]	1.303 ($^3\Delta_2$)
					2.020 ($^3\Pi_{0-}$)
B	$^3\Pi$	2.6 (1)	2.1	2.6 (1)	2.056 ($^3\Pi_{0+}$)
C	$^3\Pi$		~2.2	2.8 (1)	2.173 ($^3\Pi_1$)
D	f	3.24 (5)	2.7	3.24 (5)	
E	f	3.44 (5)	3.0	3.44 (5)	2.914 ($^1\Pi$)
F	f			3.60 (5)	
G	f			3.74 (5)	
H	g	4.05 (5)	3.60	4.05 (5)	3.585 ($^3\Phi_2$)
I	g	~4.2 (5)	3.81	~4.3	3.892 ($^3\Phi_3$)
J				~5.2	

[a]The electron configuration for HfO is $...5\sigma^2 2\pi^4 6\sigma^2 1\delta^0$ ($^1\Sigma^+$) and that for HfO^- is $...5\sigma^2 2\pi^4 6\sigma^2 1\delta^1$ ($^2\Delta$). [b]Number in the parentheses represents experimental uncertainties in the last digit. [c]Electron affinity for HfO. [d]Calculated VDE at the B3LYP level is 0.67 eV. [e]Calculated VDE at the B3LYP level is 1.90 eV. [f]These relatively weak features are likely due to the singlet $^1\Delta$ and $^1\Pi$ states. [g]Tentatively assigned to the shakeup transitions.

Table 2. Experimental Adiabatic (ADE) and Vertical (VDE) Detachment Energies from the Photoelectron Spectra of HfO_n^- (n = 2−6), Compared to the Calculated VDEs at the B3LYP Level from the Anion Ground-State and Low-Lying Isomers[a]

species	feature	ADE (expt)[b,c]	VDE (expt)[b]	state and relative energy[d]	VDE (theo)[d]
HfO_2^-	X	2.125 (10)[e]	2.125 (10)	**C_{2v} ($^2A_1$) 0.00**	**2.24**
	A		3.68 (5)		
	B		4.63 (5)		
	C		5.30 (5)		
HfO_3^-	X	3.6 (1)	3.82 (5)	**C_s ($^2A''$) 0.00**	**4.01**
	A		4.55 (5)		
	B		5.44 (5)		
HfO_4^-	X	3.67 (5)	3.84 (5)	**C_{2v} ($^2A_2$) 0.00**	**3.64**
	A		4.61 (5)	C_{2v} ($^2B_1$) 0.20	4.34
	B		5.34 (5)		
	C		5.71 (5)		
HfO_5^-	X	3.9 (1)	4.43 (10)	**C_s ($^2A''$) 0.00**	**4.12**
	A		5.14 (10)		
	B		5.30 (10)		
	C		6.00 (10)		
HfO_6^-	X	4.9 (1)	5.32 (10)	**C_s ($^4A''$) 0.00**	**4.86**
	A		5.57 (10)	**C_2 (^4A) 0.06**	**5.11**
	B		5.88 (10)	C_2 (^2A) 0.10	4.24
				C_s ($^2A''$) 0.25	4.89

[a]The calculated VDEs at the B3LYP level should be compared to the experimental ground-state VDEs. All energies are in eV. [b]Numbers in the parentheses represent experimental uncertainties in the last digits. [c]Ground-state ADE represents the electron affinity of the corresponding neutral cluster. [d]The assigned anion structures are shown in bold. [e]Two symmetric modes, 890 ± 30 and 290 ± 30 cm^{-1}, are resolved for the HfO_2 neutral ground state (band X; Figure 2a).

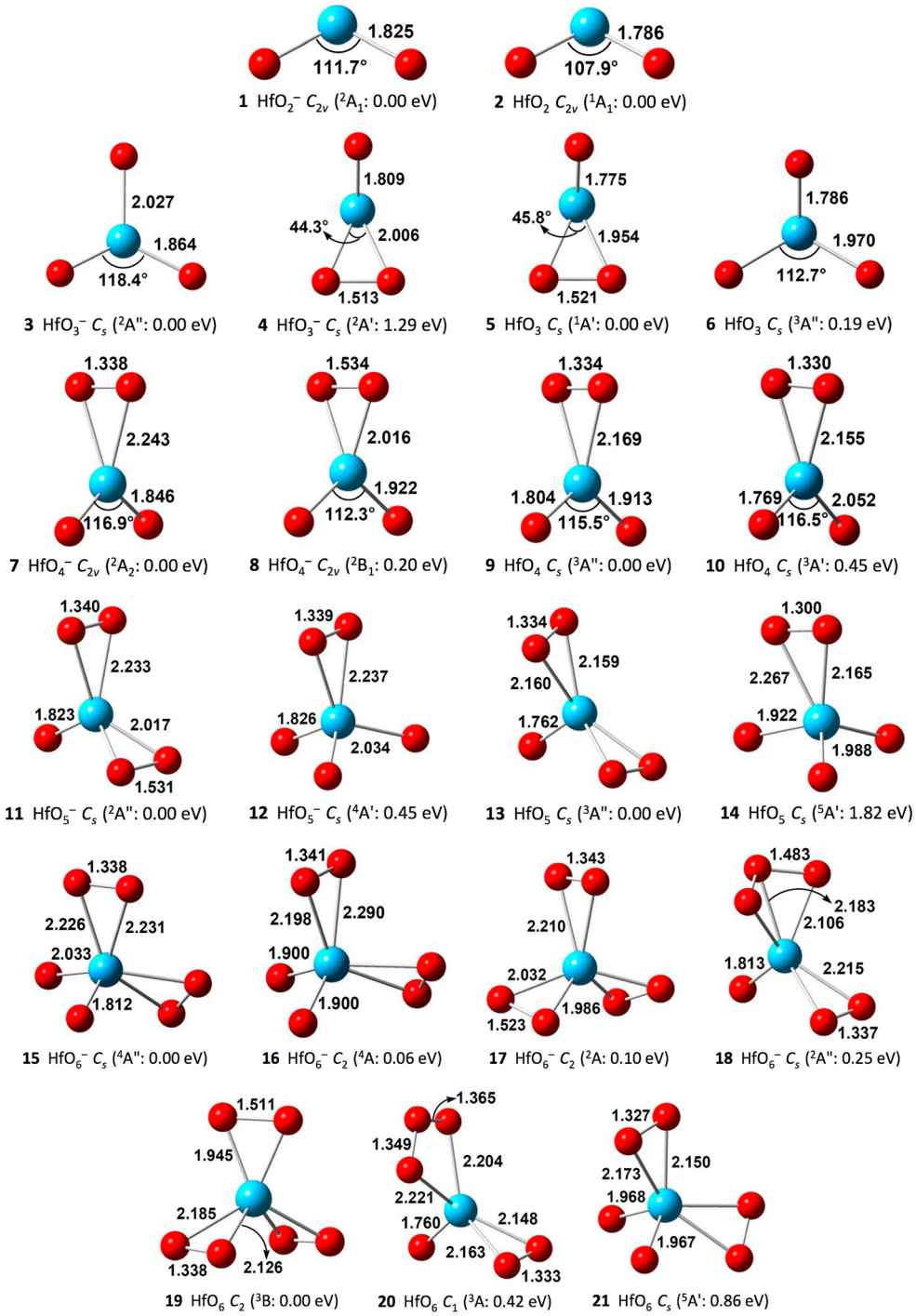

Figure 4. Optimized global minima and low-lying isomers for HfO_n^- and HfO_n (n = 2−6) at the B3LYP level of theory. Symmetries, electronic state, and relative energies for each structure are shown.

particular is shorter than typical Hf═O distances;[45] see section VI.A for additional discussion. Furthermore, the calculated Hf═O stretching frequency is 976.6 cm^{-1} (unscaled), in excellent agreement with recent gas-phase experimental data (974.09 cm^{-1}).[29]

A. HfO_2^- and HfO_2. The HfO_2^- anion adopts a bent structure, **1** (C_{2v}, $^2A_1$), with an Hf−O bond distance of 1.825 Å and ∠OHfO bond angle of 111.7°. Both the bond distance and bond angle decrease slightly in the HfO_2 neutral, **2** (C_{2v}, $^1A_1$). The above structural parameters are consistent with those from prior theoretical calculations.[31,32] Note that the current structural parameters for **2** (Hf−O, 1.786 Å; ∠OHfO, 107.9°) are in excellent agreement with those deduced from recent rotational spectral measurements (1.7764 Å; 107.51°),[29] which serve as a useful benchmark of the B3LYP method used in the current calculations. These calculated Hf−O distances help define typical Hf═O double bonds.[45]

B. HfO_3^- and HfO_3. The global minimum for HfO_3^- is **3** (C_s, $^2A''$), which possesses two Hf═O double bonds (1.864 Å) and a third elongated Hf−O bond (2.027 Å); the latter is assigned to an Hf−O• single bond between the Hf atom and an O• radical. The HfO_3^- anion structure **4** (C_s, $^2A'$) is a higher

energy isomer 1.29 eV above the ground state, which involves an Hf═O double bond (1.809 Å) and an elongated O_2 unit (1.513 Å), which is a typical peroxide complex.[46] The global minimum **5** (C_s, $^1A'$) for neutral HfO_3 turns out to closely resemble **4** for the HfO_3^- anion structurally, hinting that the extra electron in **4** is essentially nonbonding and located on Hf. Structure **5** for HfO_3 is similar to that identified previously for TiO_3.[13] Structure **6** (C_s, $^3A''$) for HfO_3 is slightly higher in energy, which features two elongated Hf−O single bonds (1.970 Å) and may be considered as a diradical ($O^\bullet + O^\bullet$).

C. HfO_4^- and HfO_4. The global minimum for HfO_4^- is **7** (C_{2v}, $^2A_2$), closely followed in energy by **8** (C_{2v}, $^2B_1$). Structure **7** possesses two Hf═O double bonds (1.846 Å) and a moderately elongated O_2 unit (1.338 Å), typical for a superoxide species.[46] In contrast, structure **8** features a peroxide unit (1.534 Å) and two moderately elongated Hf−O bonds (1.922 Å), which lie between typical Hf═O double and Hf−$O^\bullet$ single bond distances. The global minimum for neutral HfO_4 is **9** (C_s, $^3A''$), which possesses an Hf═O double bond (1.804 Å), a superoxide unit (1.334 Å), and an elongated Hf−$O^\bullet$ single bond (1.913 Å). The low-lying structure **10** (C_s, $^3A'$) shows only very minor differences from **9**.

D. HfO_5^- and HfO_5. The global minimum for the HfO_5^- anion is **11** (C_s, $^2A''$), featuring an Hf═O double bond (1.823 Å), a superoxide unit (1.340 Å), and a peroxide unit (1.531 Å). Breaking the O−O single bond in the peroxide unit in **11** formed a low-lying isomer **12** (C_s, $^4A'$), which shows two $O^\bullet$ radicals (2.034 Å) and one superoxide unit (1.339 Å). The global minimum **13** (C_s, $^3A''$) for HfO_5 neutral possesses two superoxide units (1.334 Å), similar to that identified previously for TiO_5.[13] A quintet structure **14** (C_s, $^5A'$) for HfO_5 is highly distorted and located 1.82 eV higher in energy.

E. HfO_6^- and HfO_6. Four low-lying structures are found for the HfO_6^- anion (**15**−**18**) within ∼0.3 eV. The lowest-energy structure **15** (C_s, $^4A''$) is quartet, showing two superoxide units (1.338 Å), an elongated Hf−$O^\bullet$ radical unit (2.033 Å), and a Hf═O double bond (1.812 Å). Structure **16** (C_2, ^4A) is a more symmetric version of **15**, where the Hf═O and Hf−$O^\bullet$ bonds become even and the spin is equally shared by the two O atoms. Structure **17** (C_2, ^2A) possesses one superoxide (1.343 Å) and two peroxide (1.523 Å) units. Structure **18** (C_s, $^2A''$) features a superoxide unit (1.337 Å) and an O_3 unit, and the O−O distance in the latter (1.483 Å) is close to a single bond.

The global minimum for neutral HfO_6 is **19** (C_2, ^3B), which possesses one peroxide (1.511 Å) and two superoxide (1.338 Å) units. Located 0.42 eV above the global minimum, structure **20** (C_1, ^3A) differs substantially from **19**. Structure **20** shows a typical Hf═O bond (1.760 Å), a superoxide unit (1.333 Å), and an O_3 unit, where the latter can be assigned as an ozonide radical. Both structures **19** and **20** were reported in a previous matrix IR and DFT study.[28] Structure **21** (C_s, $^5A'$) features two Hf−$O^\bullet$ radicals (1.967−1.968 Å) and two superoxide units (1.327 Å), which is an unusual tetraradical species. However, this structure is 0.86 eV above the global minimum and is not viable for experimental detection.

V. COMPARISON BETWEEN EXPERIMENT AND THEORY

The calculated ground-state VDEs from the lowest energy and low-lying HfO_n^- (n = 1−6) anion structures are compared with experimental measurements in Tables 1 and 2. The agreement between the B3LYP results and experimental data is very good. In general, it appears B3LYP overestimates the VDEs for HfO^-, HfO_2^-, and HfO_3^- by 0.1−0.2 eV, whereas it underestimates the VDEs for HfO_4^-, HfO_5^-, and HfO_6^- by 0.1−0.4 eV.

A. HfO^-. As shown in footnote *d* of Table 1, the calculated ground-state VDE for HfO^- is 0.67 eV, in good agreement with the experimental measurement of 0.60 eV. The calculated VDE for the first excited-state band (1.90 eV) is also in very good agreement with the experimental result (1.8 eV). These comparisons confirm the identified $C_{\infty v}$ ($^2\Delta$) anion ground state for HfO^-. It should be noted that the calculated higher VDEs deviate substantially from experiment, suggesting that the diatomic species are of considerable challenge for the B3LYP method. Thus, a simulation of the PES spectrum is not pursued for HfO^-.

B. HfO_n^- (n = 2−5). For the larger HfO_n^- species, we simulated their PES spectra using the calculated VDEs. The simulations were done by fitting the distribution of the calculated VDEs with unit-area Gaussian functions of 0.1 eV width, and the intensities for transitions originated from photodetachment of an electron with β versus α spin are assumed as three to one.[47] Other than this assumption, the relative intensity and width of the simulated bands are entirely due to the overlapping of multiple transitions. The simulated PES spectra of HfO_n^- (n = 2−5) based on the lowest-energy and low-lying isomers are presented in Figure 5. Each simulated PES spectrum for an assigned structure (solid black curve) is slightly shifted so that the first band maximum is aligned with the experimental spectrum. The majority of the simulated PES bands contain multiple electronic transitions that are closely spaced. For HfO_n^- (n = 2−5), the anion global minima (**1**, **3**, **7**, and **11**) are well separated energetically from the next higher lying isomer, except for n = 4, which has an isomer **8** within 0.20 eV above the ground state (Figure 4). The simulated PES spectra for the global minimum structures for HfO_n^- (n = 2−5) appear to reproduce the experimental data reasonably well (Figure 5) except for n = 2. The B3LYP level of theory underestimates the excitation energies for bands A−C of HfO_2^- by as much as 0.5−0.7 eV (Figure 5a), but the spectral pattern is in good agreement with the experiment. This behavior of DFT methods is known in the literature.[48] Note that the experimental PES spectrum of HfO_4^- (Figure 3b) is relatively sharp with no indication of presence of minor isomers. We see that the simulated PES spectrum for the low-lying structure **8** of HfO_4^- (Figure 5d) deviates substantially from the experimental data and, thus, this isomeric species can be safely ruled out, suggesting that the B3LYP energetics is probably accurate up to ∼0.2 eV for the HfO_n^- clusters. Overall, the good agreement between experiment and theory lends considerable credence to the identified anion ground-state structures for HfO_n^- (n = 2−5).

C. HfO_6^-. The HfO_6^- cluster is a more complicated case. As shown in Figure 4, three low-lying structures (**15**−**17**) are identified within ∼0.1 eV, which are practically degenerate and energetically indistinguishable. Among their simulated PES spectra, the top two, **15** (C_s, $^4A''$) (Figure 6a) and **16** (C_2, ^2A) (Figure 6b), match the experimental data equally well, and both structures are likely to contribute to the experimental PES spectrum. This explains why the observed PES spectrum is so congested. The simulated spectra for isomers **17** (C_2, ^2A) (Figure 6c) and **18** (C_s, $^2A''$) (Figure 6d) disagree with the observed PES data and can be ruled out.

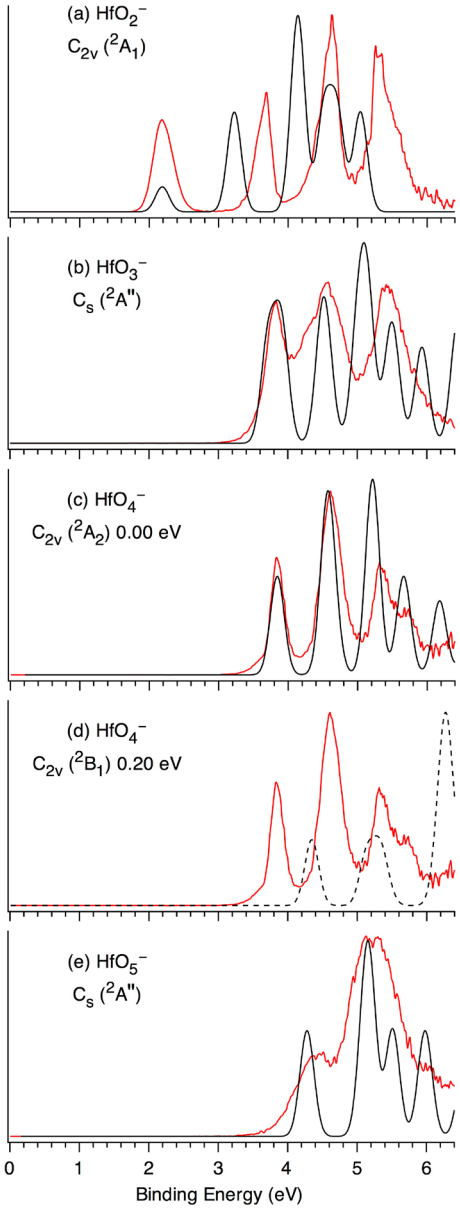

Figure 5. Simulated photoelectron spectra from the lowest-energy isomers (solid black curves) for HfO_n^- (n = 2−5), compared with the 193 nm experimental spectra (red curves) (a, b, c, e). Simulation from a low-lying C_{2v} ($^2B_1$, 0.20 eV) structure is also shown for HfO_4^- (dashed black curve) (d). The simulated solid black curves have been slightly shifted so that the first band maximum is aligned with experimental spectrum. The dashed curve represents a simulation that deviates substantially from the experimental data.

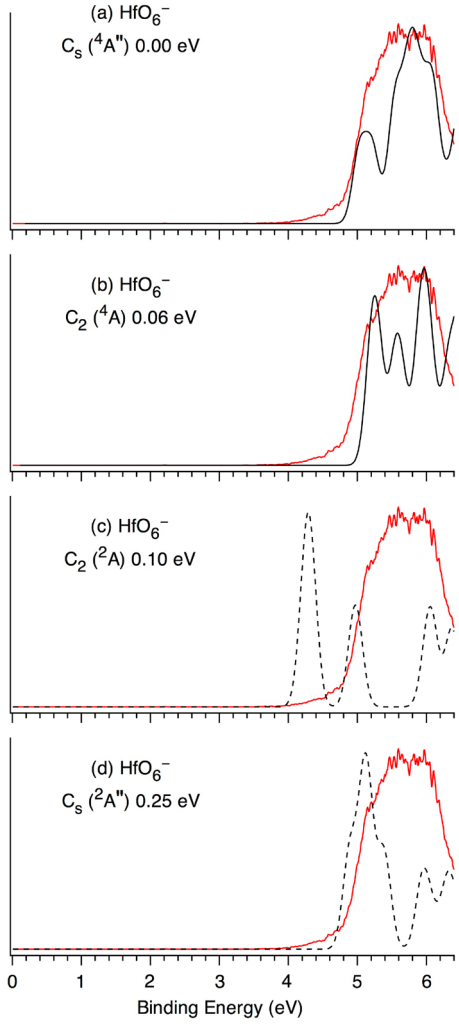

Figure 6. Simulated photoelectron spectra of HfO_6^- from the low-lying anion structures, compared with the 193 nm experimental spectrum (red curve). The simulated solid black curves (a, b) have been slightly shifted so that the first band maximum is aligned with experimental spectrum. The dashed curves represent simulations that deviate substantially from the experimental data.

VI. DISCUSSION

As shown in Figure 4, the Hf−O bond distances between Hf and an isolated O atom center at ∼1.83 and ∼2.03 Å for the anions and ∼1.77 and ∼1.91 Å for the neutrals, where the shorter Hf−O bond can be assigned to an Hf═O double bond and the longer distance to an Hf−O• single bond (associated with an O• radical). The Hf−O distances between Hf and an O_2 unit center around ∼2.02 and ∼2.23 Å for the anions and ∼1.95 and ∼2.16 Å for the neutrals, where the shorter distances are assigned to Hf−O single bonds associated with peroxo unit (O−O distance: ∼1.52 Å) and the longer distances to Hf−O half bonds associated with superoxo unit (O−O distance: ∼1.34 Å). These analyses[45,46] led the well-defined valence bond descriptions for the global minimum structures of HfO_n^- and HfO_n, as depicted in Figure 7.

A. Electronic States of HfO. As mentioned in section V, the diatomic HfO^- and HfO species pose considerable challenges for the B3LYP method. We thus intend to analyze the electronic states of HfO only qualitatively with the aid of B3LYP calculations. The HfO neutral cluster possesses the $C_{\infty v}$ ($^1\Sigma^+$) ground state with a closed-shell electron configuration of $...5\sigma^2 2\pi^4 6\sigma^2 1\delta^0$. The 5σ molecular orbital (MO) is a bonding orbital composed of 48% O 2p and 41% Hf 5d/6s atomic orbitals (AOs), whereas the degenerate 2π MOs are π bonding in nature that are composed of predominant O 2p (73%) and minor Hf 5d (23%) AOs. The 6σ MO is essentially nonbonding dominated by the Hf 6s AO (86%). The above analysis reveals certain triple bond character in HfO, but the bond order may be effectively viewed as two because the π MOs are relatively weak (with partial O 2p lone pair character). It is noted that, consistent with the above "triple bond" description, the measured bond distance of HfO (1.7231481 Å)[29] and that calculated in the current study (1.729 Å) appear to be shorter

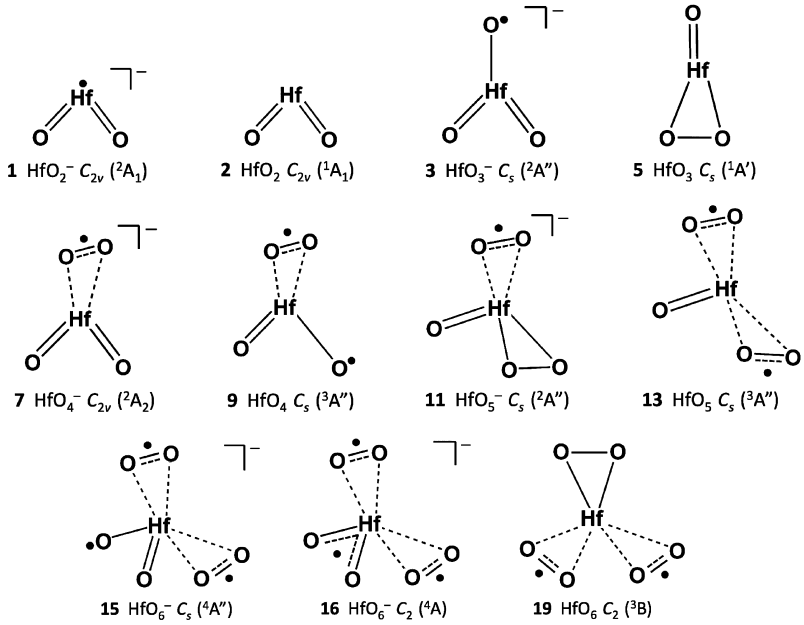

Figure 7. Valence bond descriptions for the global minima and selected low-lying structures of HfO_n^- and HfO_n (n = 2−6). The dashed line represents a formal bond order of 0.5. The isomer numbering is the same as in Figure 4.

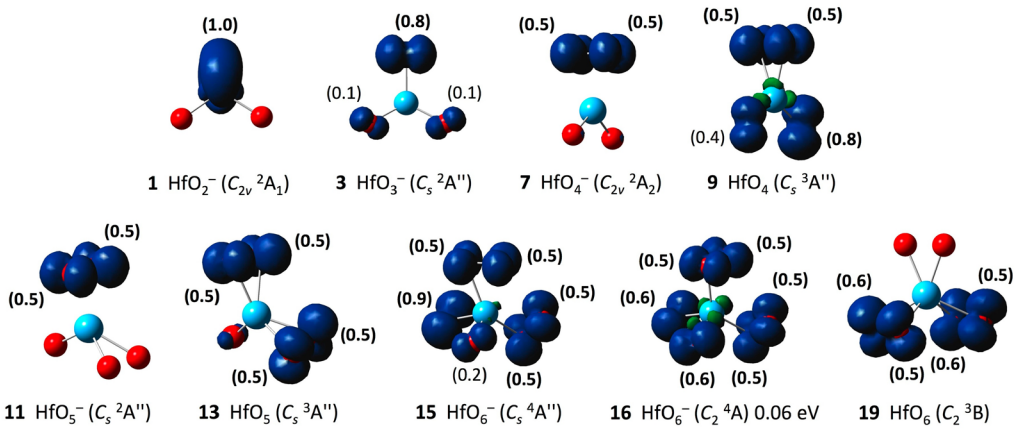

Figure 8. Spin densities (in lel) for the global minima and selected low-lying structures of HfO_n^- and HfO_n (n = 2−6). The isomer numbering is the same as in Figure 4.

than those calculated for the rest of clusters with typical Hf═O double bonds (Figure 4).

In the $C_{\infty v}$ ($^2\Delta$) ground state of the HfO^- anion, the extra electron occupies the 1δ MO, which is completely nonbonding with pure Hf 5d character (100%). Photodetachment from the 1δ MO of the HfO^- anion generates the $^1\Sigma^+$ neutral ground state with a calculated VDE of 0.67 eV, which is in excellent agreement with the experimental value of 0.60 eV (Figure 1 and Table 1). Interestingly, the measured electron affinity of HfO (0.5 eV) is markedly lower than that of TiO (1.30 eV).[24] This may be attributed to the strong relativistic effects of the 5d elements, which destabilize the 1δ MO in the HfO^- anion. Thus, the HfO^- and HfO species are expected to be more reactive toward oxygen relative to TiO^- and TiO.

The next detachment channel involves the removal of the β electron from the 6σ MO, which results in the triplet $^3\Delta$ neutral state with a predicted VDE of 1.90 eV as compared to the experimental value of 1.8 eV (band A). The spin−orbit components of the $^3\Delta$ state ($^3\Delta_1$, $^3\Delta_2$, $^3\Delta_3$) are expected to be closely spaced due to the predominant Hf 6s nature of the MO and thus are not resolved in Figure 1. The next major PES bands B and C are tentatively assigned to the $^3\Pi$ states ($^3\Pi_0$, $^3\Pi_1$, $^3\Pi_2$), which are associated with the removal of the β electrons from the 2π MOs. The corresponding singlet $^1\Delta$ and $^1\Pi$ states due to the removal of the α electrons from the 6σ and 2π MOs, respectively, are anticipated to be weaker in intensities,[47] and these are tentatively assigned to the observed bands D−G. Shake-up transitions may also contribute to the weak D−I bands. Finally, the broad band J at ∼5.2 may be due to electron detachment from the 5σ bonding MO, which is predicted at 5.00−5.03 eV at the B3LYP level. Extensive vibrational excitation is expected due to the strong bonding nature of the 5σ MO. The above assignments are in overall agreement with the most recent analysis of the high-resolution optical spectra of HfO, whose term scheme is still a topic of discussion in the literature.[49] In Table 1, we have listed the term values for numerous electronic transitions based on the current PES measurements, compared with the prior optical spectroscopic data.

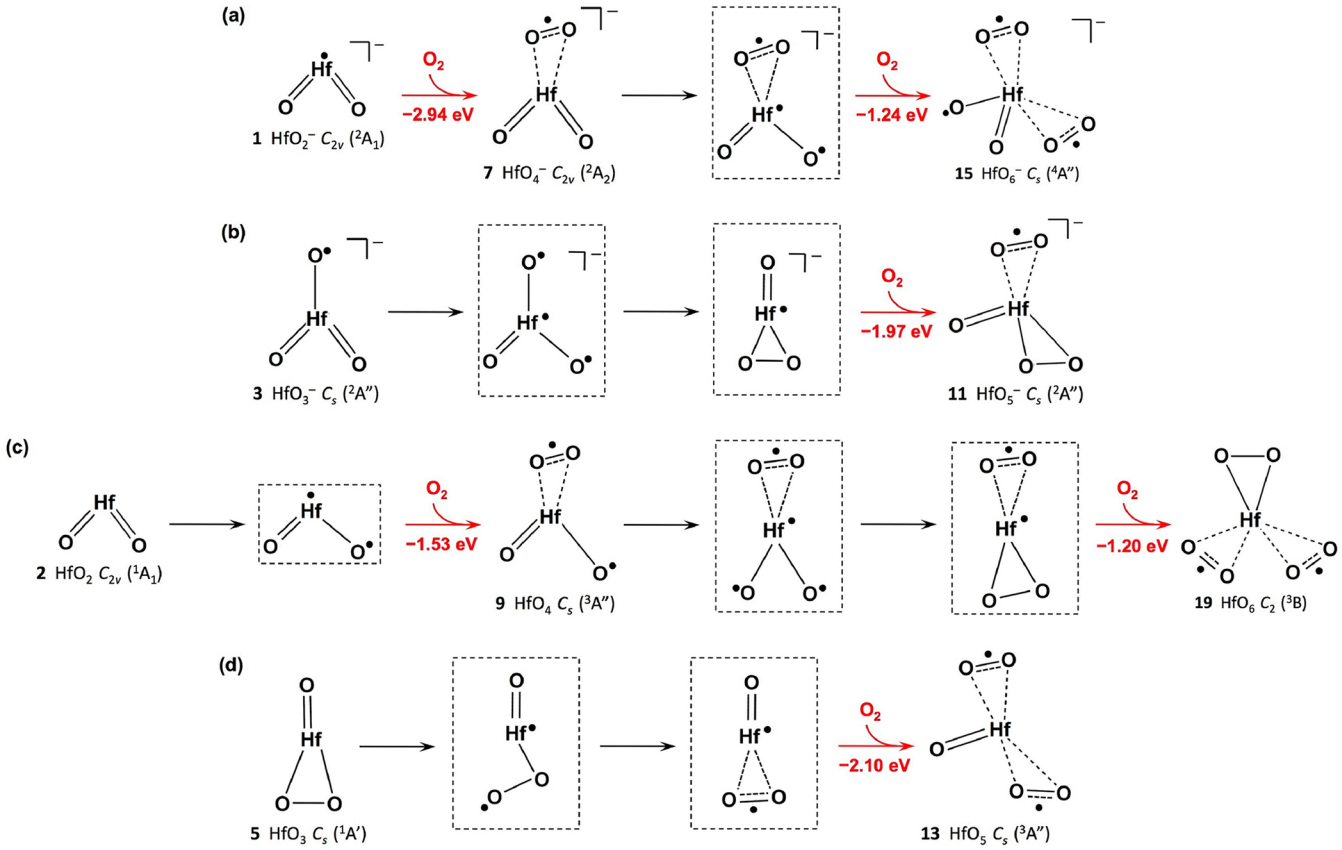

Figure 9. Schematics describing O_2 adsorption and activation on the Hf centers. A reaction may involve certain proposed intermediate states (shown in dashed squares) and the overall adsorption energy from the initial to final states at the B3LYP level is shown.

B. HfO_2^- and HfO_2. HfO_2 is the smallest stoichiometric Hf oxide cluster, in which both Hf and O assume their favorite 4+ and 2− formal oxidation states, respectively, and all Hf 6s/5d electrons are transferred to O. In the HfO_2^- anion, the extra electron occupies the Hf 6s/5d based HOMO of the anion (Figure 8), whose detachment produces the vibrationally resolved neutral ground-state band X (Figure 2a) at a VDE of 2.125 ± 0.010 eV (Table 2). A recent benchmarking theoretical study by Li and Dixon[32] yielded a ground-state VDE of 2.23 eV for HfO_2^- at the CCSD(T) level, in good agreement with the experiment (and with the current B3LYP result: 2.24 eV). Of the two vibrational modes observed, the higher one (890 ± 30 cm^{-1}, compared to 883.4 cm^{-1} in matrix IR measurements[27]) is assigned to the Hf═O stretch and the lower one (290 ± 30 cm^{-1}) to the O−Hf−O bending. Indeed, upon electron detachment, the anion-to-neutral geometric changes between HfO_2^- (**1**) and HfO_2 (**2**) involve the shortening of the Hf═O bond distance by ∼0.04 Å and the shrinking of ∠OHfO bond angle by ∼4° (Figure 4). Thus, both the symmetric Hf═O stretching and O−Hf−O bending modes are expected to be active accompanying the photodetachment. Our B3LYP calculations predict the frequencies for the symmetric stretching and bending modes to be 906.8 and 292.9 cm^{-1} (unscaled), respectively, in good agreement with the experiment. A prior B3LYP/SBKJ calculation predicted the corresponding stretching and bending modes to be 898 and 293 cm^{-1}, respectively.[30]

Band A in the PES spectrum of HfO_2^- (Figure 2) corresponds to electron detachment from the O 2p based HOMO−1. The binding energy difference between band X and A is equivalent to the promotion of an electron from the HOMO to the lowest unoccupied molecular orbital (LUMO) in neutral HfO_2. This gap is evaluated from the ADE difference of the X and A bands as 1.3 eV. Li and Dixon predicted a value of 1.51 eV for this energy gap at CCSD(T) level.[32] As shown in Figure 5a, the current B3LYP result significantly underestimates this energy gap.

It is interesting to compare HfO_2^- with its isovalent 3d counterpart, TiO_2^-. HfO_2^- has a substantially higher ADE for the Hf 6s/5d derived band X (2.125 eV) and lower ADE for the O 2p derived band A (3.44 eV) relative to those of TiO_2^- (1.59 and 3.81 eV),[15] resulting in a reduced X−A energy gap in HfO_2^- (1.3 eV for HfO_2^- versus 2.2 eV for TiO_2^-). In contrast, HfO_2 bulk oxide possesses a significantly wider band gap (∼5.7 eV)[25] than TiO_2 (rutile: ∼3.0 eV; anatase: ∼3.2 eV).[23] The energy gap observed in the monomeric HfO_2 is thus surprisingly small, which represents only ∼23% of the bulk band gap, whereas the energy gap in the monomeric TiO_2 is already ∼70% of the bulk band gap. The origin for this difference may be partly attributed to the lower electronegativity for Hf (1.30 at the Pauling scale versus 1.54 for Ti), which results in larger charge transfer from Hf to O.[50,51] In addition, MO analysis shows that the SOMO of HfO_2^- (Figure 8) is a mixture of Hf 6s (43%) and 5d (37%) AOs, in which the strong involvement of Hf 6s may help stabilize the SOMO due to the relativistic effect, further reducing the energy gap in the HfO_2^- monomer.

C. Oxygen-Rich HfO_n^- and HfO_n (n = 3−6) Clusters: Oxygen Radicals, Superoxides, Peroxides, Diradicals, and Triradicals. Valence bond descriptions for the O-rich

HfO_n^- and HfO_n (n = 3−6) clusters are presented in Figure 7, where all anion clusters (**3**, **7**, **11**, **15**, and **16**) are observed experimentally (Figures 5 and 6) and the neutral structures (**5**, **9**, **13**, and **19**) are clearly the global minima on their potential energy surfaces at the B3LYP level. A survey of these structures reveals a variety of active oxygen species, such as the $O^\bullet$ radicals (**3**, **9**, and **15**), the $O_2^\bullet$ superoxides (**7**, **9**, **11**, **13**, **15**, **16**, and **19**), and the peroxides (**5**, **11**, and **19**). The combinations of $O^\bullet$ radical and/or $O_2^\bullet$ superoxide lead to the diradical complexes for **9**, **13**, and **19**. The $O^\bullet$ and $O_2^\bullet$ radical nature of these clusters is further supported by the spin density analyses, as depicted in Figure 8.

Interestingly, structures **15** and **16** of HfO_6^- show triradical characters, each possessing one $O^\bullet$ radical and two $O_2^\bullet$ superoxide units. The subtle differences between them are that the Hf−$O^\bullet$ single and Hf═O double bonds in **15** are localized, whereas these bonds are delocalized in **16** with a formal bond order of 1.5 each and consequently the unpaired spin is shared equally by the two O atoms. The triradical nature of HfO_6^- appears to have an observable stabilization effect. Among the O-rich HfO_n^- (n = 3−6) clusters, HfO_3^-, HfO_4^-, and HfO_5^- possess roughly the same ADEs (3.6−3.9 eV; Table 2), whereas the ADE shows an abrupt increase at HfO_6^- (4.9 eV). This may lead to distinctly different surface and chemical properties for each Hf center.

Oxygen radicals and superoxides are widely discussed in the oxide surface chemistry[1] and in transition metal oxide clusters.[3−9] Diradicals are relatively rare in oxide cluster complexes,[9−13,28] whereas the $Ti_4O_{10}^-$, $Sc(O_2)_3$, and $Al(O_2)_3$ clusters are probably the only triradical oxide species observed so far.[12,14,52] It is remarkable that in the HfO_n^- and HfO_n (n = 3−6) clusters all oxygen radicals, superoxides, peroxides, diradicals, and triradicals are attached to a single Hf center. These clusters appear to be structurally rather flexible to accommodate the appropriate amount of oxygen. Effectively, the sum of the formal Hf−O bond orders around the Hf center is equal to four and five, respectively, for the neutral and anion clusters (Figure 7). These values match the number of available 5d/6s valence electrons around the Hf center (four for Hf versus five for Hf^-), with the HfO_2^- anion being the exception due to a "residual" 5d/6s electron on the Hf center. Interestingly, an $Hf(O_2)_4$ species was characterized recently in matrix IR experiments,[28] which may be viewed to contain four superoxide units.

D. Molecular Models for O_2 Activation on the Hf Center. The HfO_n^- and HfO_n (n = 2−6) clusters offer opportunities to model the interactions between the Hf center and O_2. Figure 9 depicts schematically the selected routes for the interconversions between these clusters via O_2 adsorption. Most of these processes require intermediate states (shown in dashed squares), which primarily involve the promotion of an electron from O 2p to Hf 5d/6s orbitals. Once such an energy barrier is overcome, the O_2 adsorption takes place readily, resulting in a substantial overall adsorption energy (final versus initial states) for each adsorption process. The O_2 adsorption energy ranges from −1.20 to −2.94 eV at the current level of theory, suggesting strong chemisorption interactions. As a consequence, each adsorption reaction activates an O_2 molecule to a superoxide and concurrently generates additional activated oxygen species, such as $O^\bullet$ radical, superoxide, and peroxide. Similar oxygen species may also be stabilized around Hf centers on oxide surfaces, which may play critical roles in its surface chemistry and photochemistry.

VII. CONCLUSIONS

We have investigated the electronic and geometric structures and chemical bonding of a series of monohafnium oxide clusters, HfO_n^- and HfO_n (n = 1−6), using anion photoelectron spectroscopy and density-functional calculations at the B3LYP level. Electron affinities are obtained for all the HfO_n species. Activated oxygen species such as radical, superoxide, peroxide, diradical, and triradical are identified in these clusters. The Hf center is shown to be highly flexible to accommodate oxygen species, and the sum of the formal Hf−O bond orders around the Hf center is equal to four and five for all of the neutral and anion clusters, respectively. The O-rich HfO_n^- and HfO_n (n = 3−6) clusters are used to model O_2 adsorption and activation at the Hf center. Both neutral and anion clusters are shown to interact strongly with O_2.

■ AUTHOR INFORMATION

Corresponding Author

*E-mail: X.H., xhuang@fzu.edu.cn; L.-S.W., Lai-Sheng_Wang@brown.edu.

Notes

The authors declare no competing financial interest.

■ ACKNOWLEDGMENTS

This work was supported by the Chemical Sciences, Geosciences and Biosciences Division, Office of Basic Energy Sciences, U.S. Department of Energy, under grant No. DE-FG02-03ER15481 (catalysis center program). X.H. gratefully acknowledges supports from the Natural Science Foundation of China (21071031 and 90922022).

■ ADDITIONAL NOTE

During the review of this manuscript, a related paper on the photoelectron spectroscopy of the diatomic HfO^- anion at a lower photon energy appeared,[53] which is in agreement with the current work.

■ REFERENCES

(1) (a) Che, M.; Tench, A. J. *Adv. Catal.* **1982**, *31*, 77−133. (b) Che, M.; Tench, A. J. *Adv. Catal.* **1983**, *32*, 1−148.

(2) (a) Bohme, D. K.; Schwarz, H. *Angew. Chem. Int. Ed.* **2005**, *44*, 2336−2354. (b) Asmis, K. R.; Sauer, J. *Mass Spect. Rev.* **2007**, *26*, 542−562. (c) Johnson, G. E.; Mitrić, R.; Bonačić-Koutecký, V.; Castleman, A. W., Jr. *Chem. Phys. Lett.* **2009**, *475*, 1−9. (d) Gong, Y.; Zhou, M. F.; Andrews, L. *Chem. Rev.* **2009**, *109*, 6765−6808. (e) Zhai, H. J.; Wang, L. S. *Chem. Phys. Lett.* **2010**, *500*, 185−195. (f) Zhao, Y. X.; Wu, X. N.; Ma, J. B.; He, S. G.; Ding, X. L. *Phys. Chem. Chem. Phys.* **2011**, *13*, 1925−1938.

(3) Fielicke, A.; Meijer, G.; von Helden, G. *J. Am. Chem. Soc.* **2003**, *125*, 3659−3667.

(4) (a) Justes, D. R.; Mitrić, R.; Moore, N. A.; Bonačić-Koutecký, V.; Castleman, A. W., Jr. *J. Am. Chem. Soc.* **2003**, *125*, 6289−6299. (b) Johnson, G. E.; Mitrić, R.; Tyo, E. C.; Bonačić-Koutecký, V.; Castleman, A. W., Jr. *J. Am. Chem. Soc.* **2008**, *130*, 13912−13920. (c) Johnson, G. E.; Mitrić, R.; Nößler, M.; Tyo, E. C.; Bonačić-Koutecký, V.; Castleman, A. W., Jr. *J. Am. Chem. Soc.* **2009**, *131*, 5460−5470. (d) Nößler, M.; Mitrić, R.; Bonačić-Koutecký, V.; Johnson, G. E.; Tyo, E. C.; Castleman, A. W., Jr. *Angew. Chem. Int. Ed.* **2010**, *49*, 407−410.

(5) (a) Feyel, S.; Döbler, J.; Schröder, D.; Sauer, J.; Schwarz, H. *Angew. Chem. Int. Ed.* **2006**, *45*, 4681−4685. (b) Santambrogio, G.; Brümmer, M.; Wöste, L.; Döbler, J.; Sierka, M.; Sauer, J.; Meijer, G.; Asmis, K. R. *Phys. Chem. Chem. Phys.* **2008**, *10*, 3992−4005.

(6) (a) Dong, F.; Heinbuch, S.; Xie, Y.; Rocca, J. J.; Bernstein, E. R.; Wang, Z. C.; Deng, K.; He, S. G. *J. Am. Chem. Soc.* **2008**, *130*, 1932−1943. (b) Zhao, Y. X.; Wu, X. N.; Wang, Z. C.; He, S. G.; Ding, X. L. *Chem. Commun.* **2010**, *46*, 1736−1738. (c) Ma, J. B.; Wu, X. N.; Zhao, Y. X.; Ding, X. L.; He, S. G. *J. Phys. Chem. A* **2010**, *114*, 10024−10027.
(7) Gong, Y.; Zhou, M. F.; Tian, S. X.; Yang, J. L. *J. Phys. Chem. A* **2007**, *111*, 6127−6130.
(8) Huang, X.; Zhai, H. J.; Waters, T.; Li, J.; Wang, L. S. *Angew. Chem. Int. Ed.* **2006**, *45*, 657−660.
(9) Zhai, H. J.; Zhang, X. H.; Chen, W. J.; Huang, X.; Wang, L. S. *J. Am. Chem. Soc.* **2011**, *133*, 3085−3094.
(10) Zhai, H. J.; Kiran, B.; Cui, L. F.; Li, X.; Dixon, D. A.; Wang, L. S. *J. Am. Chem. Soc.* **2004**, *126*, 16134−16141.
(11) Zhao, Y. X.; Yuan, J. Y.; Ding, X. L.; He, S. G.; Zheng, W. J. *Phys. Chem. Chem. Phys.* **2011**, *13*, 10084−10090.
(12) Janssens, E.; Santambrogio, G.; Brümmer, M.; Wöste, L.; Lievens, P.; Sauer, J.; Meijer, G.; Asmis, K. R. *Phys. Rev. Lett.* **2006**, *96*, 233401 (4 pages).
(13) Gong, Y.; Zhou, M. F. *J. Phys. Chem. A* **2008**, *112*, 9758−9762.
(14) Gong, Y.; Ding, C. F.; Zhou, M. F. *J. Phys. Chem. A* **2007**, *111*, 11572−11578.
(15) Zhai, H. J.; Wang, L. S. *J. Am. Chem. Soc.* **2007**, *129*, 3022−3026.
(16) (a) Zhai, H. J.; Döbler, J.; Sauer, J.; Wang, L. S. *J. Am. Chem. Soc.* **2007**, *129*, 13270−13276. (b) Zhai, H. J.; Li, S. G.; Dixon, D. A.; Wang, L. S. *J. Am. Chem. Soc.* **2008**, *130*, 5167−5177.
(17) (a) Zubarev, D. Yu.; Averkiev, B. B.; Zhai, H. J.; Wang, L. S.; Boldyrev, A. I. *Phys. Chem. Chem. Phys.* **2008**, *10*, 257−267. (b) Huang, X.; Zhai, H. J.; Kiran, B.; Wang, L. S. *Angew. Chem, Int. Ed.* **2005**, *44*, 7251−7254. (c) Zhai, H. J.; Averkiev, B. B.; Zubarev, D. Yu.; Wang, L. S.; Boldyrev, A. I. *Angew. Chem. Int. Ed.* **2007**, *46*, 4277−4280. (d) Zhai, H. J.; Chen, W. J.; Huang, X.; Wang, L. S. *RSC Adv.* **2012**, *2*, 2707−2712.
(18) Waters, T.; O'Hair, R. A. J.; Wedd, A. G. *J. Am. Chem. Soc.* **2003**, *125*, 3384−3396.
(19) Molek, K. S.; Jaeger, T. D.; Duncan, M. A. *J. Chem. Phys.* **2005**, *123*, 144313 (10 pages).
(20) (a) Wyrwas, R. B.; Yoder, B. L.; Maze, J. T.; Jarrold, C. C. *J. Phys. Chem. A* **2006**, *110*, 2157−2164. (b) Mayhall, N. J.; Rothgeb, D. W.; Hossain, E.; Raghavachari, K.; Jarrold, C. C. *J. Chem. Phys.* **2009**, *130*, 124313 (10 pages).
(21) (a) Gutsev, G. L.; Jena, P.; Zhai, H. J.; Wang, L. S. *J. Chem. Phys.* **2001**, *115*, 7935−7944. (b) Zhai, H. J.; Wang, L. S. *J. Chem. Phys.* **2002**, *117*, 7882−7888. (c) Zhai, H. J.; Huang, X.; Cui, L. F.; Li, X.; Li, J.; Wang, L. S. *J. Phys. Chem. A* **2005**, *109*, 6019−6030. (d) Zhai, H. J.; Huang, X.; Waters, T.; Wang, X. B.; O'Hair, R. A. J.; Wedd, A. G.; Wang, L. S. *J. Phys. Chem. A* **2005**, *109*, 10512−10520. (e) Huang, X.; Zhai, H. J.; Li, J.; Wang, L. S. *J. Phys. Chem. A* **2006**, *110*, 85−92. (f) Zhai, H. J.; Wang, L. S. *J. Chem. Phys.* **2006**, *125*, 164315. (9 pages). (g) Zhai, H. J.; Wang, B.; Huang, X.; Wang, L. S. *J. Phys. Chem. A* **2009**, *113*, 3866−3875. (h) Zhai, H. J.; Wang, B.; Huang, X.; Wang, L. S. *J. Phys. Chem. A* **2009**, *113*, 9804−9813. (i) Li, S. G.; Zhai, H. J.; Wang, L. S.; Dixon, D. A. *J. Phys. Chem. A* **2009**, *113*, 11273−11288. (j) Chen, W. J.; Zhai, H. J.; Zhang, Y. F.; Huang, X.; Wang, L. S. *J. Phys. Chem. A* **2010**, *114*, 5958−5966. (k) Chen, W. J.; Zhai, H. J.; Huang, X.; Wang, L. S. *Chem. Phys. Lett.* **2011**, *512*, 49−53. (l) Li, S. G.; Zhai, H. J.; Wang, L. S.; Dixon, D. A. *J. Phys. Chem. A* **2012**, *116*, 5256−5271.
(22) Trunschke, A.; Hoang, D. L.; Radnik, J.; Brzezinka, K.-W.; Brückner, A.; Lieske, H. *Appl. Catal., A* **2001**, *208*, 381−392.
(23) (a) Diebold, U. *Surf. Sci. Rep.* **2003**, *48*, 53−229. (b) Thompson, T. L.; Yates, J. T., Jr. *Chem. Rev.* **2006**, *106*, 4428−4453.
(24) Wu, H.; Wang, L. S. *J. Chem. Phys.* **1997**, *107*, 8221−8228.
(25) Wilk, G. D.; Wallace, R. M.; Anthony, J. M. *J. Appl. Phys.* **2001**, *89*, 5243−5275.
(26) Rauh, E. G.; Ackermann, R. J. *J. Chem. Phys.* **1974**, *60*, 1396−1400.
(27) (a) Chertihin, G. V.; Andrews, L. *J. Phys. Chem.* **1995**, *99*, 6356−6366. (b) Gong, Y.; Zhang, Q. Q.; Zhou, M. F. *J. Phys. Chem. A* **2007**, *111*, 3534−3539.
(28) Gong, Y.; Zhou, M. F. *J. Phys. Chem. A* **2007**, *111*, 8973−8979.
(29) Lesarri, A.; Suenram, R. D.; Brugh, D. *J. Chem. Phys.* **2002**, *117*, 9651−9662.
(30) Zheng, W.; Bowen, K. H., Jr.; Li, J.; Dabkowska, I.; Gutowski, M. *J. Phys. Chem. A* **2005**, *109*, 11521−11525.
(31) Woodley, S. M.; Hamad, S.; Mejias, J. A.; Catlow, C. R. A. *J. Mater. Chem.* **2006**, *16*, 1927−1933.
(32) Li, S. G.; Dixon, D. A. *J. Phys. Chem. A* **2010**, *114*, 2665−2683.
(33) (a) Wang, L. S.; Cheng, H. S.; Fan, J. *J. Chem. Phys.* **1995**, *102*, 9480−9493. (b) Wang, L. S.; Wu, H. In *Advances in Metal and Semiconductor Clusters, Vol. 4, Cluster Materials*; Duncan, M. A., Ed.; JAI Press: Greenwich, CT, 1998; pp 299−343.
(34) (a) Wang, L. S.; Li, X. In *Clusters and Nanostructure Interfaces*; Jena, P., Khanna, S. N., Rao, B. K., Eds.; World Scientific: Singapore, 2000; pp 293−300. (b) Akola, J.; Manninen, M.; Häkkinen, H.; Landman, U.; Li, X.; Wang, L. S. *Phys. Rev. B* **1999**, *60*, R11297−R11300. (c) Wang, L. S.; Li, X.; Zhang, H. F. *Chem. Phys.* **2000**, *262*, 53−63. (d) Zhai, H. J.; Wang, L. S.; Alexandrova, A. N.; Boldyrev, A. I. *J. Chem. Phys.* **2002**, *117*, 7917−7924.
(35) Becke, A. D. *J. Chem. Phys.* **1993**, *98*, 1372−1377.
(36) Lee, C.; Yang, W.; Parr, R. G. *Phys. Rev. B* **1988**, *37*, 785−789.
(37) Stephens, P. J.; Devlin, F. J.; Chabalowski, C. F.; Frisch, M. J. *J. Phys. Chem.* **1994**, *98*, 11623−11627.
(38) Andrae, D.; Haeussermann, U.; Dolg, M.; Stoll, H.; Preuss, H. *Theor. Chim. Acta* **1990**, *77*, 123−141.
(39) Küchle, W.; Dolg, M.; Stoll, H.; Preuss, H. *Pseudopotentials of the Stuttgart/Dresden Group 1998*, revision August 11, 1998 (http://www.theochem.uni-stuttgart.de/pseudopotentials).
(40) Martin, J. M. L.; Sundermann, A. *J. Chem. Phys.* **2001**, *114*, 3408−3420.
(41) Dunning, T. H., Jr. *J. Chem. Phys.* **1989**, *90*, 1007−1023.
(42) Kendall, R. A.; Dunning, T. H., Jr.; Harrison, R. J. *J. Chem. Phys.* **1992**, *96*, 6796−6806.
(43) Tozer, D. J.; Handy, N. C. *J. Chem. Phys.* **1998**, *109*, 10180−10189.
(44) Frisch, M. J.; Trucks, G. W.; Schlegel, H. B.; Scuseria, G. E.; Robb, M. A.; Cheeseman, J. R.; Montgomery, J. A., Jr.; Vreven, T.; Kudin, K. N.; Burant, J. C.; et al. *Gaussian 03*, revision D.01; Gaussian, Inc.: Wallingford, CT, 2004.
(45) On the basis of the current DFT calculations (Figure 4), the Hf−O bond distances in the HfO_n^- and HfO_n clusters appear to be well correlated with the bond order, which yet show moderate charge-state dependence. In short, the Hf═O (double), Hf—O (single), and Hf···O (half) bond distances in the neutral clusters center at 1.77, 1.91−1.95, and 2.16 Å, respectively. In the anion clusters, the values are 1.83, 2.02−2.03, and 2.23 Å.
(46) Superoxide and peroxide are well-defined chemical species, which correspond to O_2^- (∼1.33 Å) and O_2^{2-} (∼1.49 Å) with a formal bond order of 1.5 and 1.0, respectively; see, for example, ref 1. These values are to be compared to the bond distance of ∼1.21 Å and the formal bond order of 2.0 in the dioxygen molecule (O_2).
(47) See, for example: Cox, P. A.; Orchard, F. A. *Chem. Phys. Lett.* **1970**, *7*, 273−275.
(48) Pacchioni, G. *J. Chem. Phys.* **2008**, *128*, 182505 (10 pages).
(49) (a) Jonsson, J.; Edvinsson, G.; Taklif, A. G. *J. Mol. Spectrosc.* **1995**, *172*, 299−301. (b) Kaledin, L. A.; McCord, J. E.; Heaven, M. C. *J. Mol. Spectrosc.* **1995**, *173*, 37−43.
(50) Brünken, S.; Müller, H. S. P.; Menten, K. M.; McCarthy, M. C.; Thaddeus, P. *Astrophys. J.* **2008**, *676*, 1367−1371.
(51) Prior comparative calculations on MO_2 (M = Ti, Hf) clusters at the B3LYP level by Li and Dixon[32] showed that the natural charges on the metal center are +2.02 |e| for HfO_2, as compared to +1.52 |e| for TiO_2. This should override their difference in M═O bond distances (1.7764 ± 0.0004 Å for HfO_2 versus 1.651 Å for TiO_2),[29,50] resulting in larger Coulomb repulsion in HfO_2. A similar effect is anticipated for their anions.
(52) Stößer, G.; Schnöckel, H. *Angew. Chem. Int. Ed.* **2005**, *44*, 4261−4264.

(53) Li, X.; Zheng, W.; Buonaugurio, A.; Buytendyk, A.; Bowen, K.; Balasubramanian, K. *J. Chem. Phys.* **2012**, *136*, 154306 (5 pages).